7 Particle Physics at DESY/HERA (H1)

S. Egli (until August 1999), I. Foresti, S. Hengstmann, M. Hildebrandt, N. Keller,
P. Robmann, F. Sefkow, U. Straumann, P. Truöl,
S. von Dombrowski (until July 99), R. Wallny and T. Walter

in collaboration with:
Institut für Teilchenphysik der ETH, Zürich (R. Eichler, W. Erdmann, C. Grab, M. Hilgers, H.-C. Kästli, B. List, S. Lüders, and A. Schöning), Paul–Scherrer–Institut, Villigen (S. Egli (since September 1999), K. Gabathuler, J. Gassner, and R. Horisberger), and 34 institutes outside Switzerland

(**H1**–Collaboration)

7.1 Electron proton collisions at 300 GeV center of mass energy: overall status of the project

During the first part of 1999, until the end of April, the HERA electron/positron-proton storage ring operated with electrons. A total luminosity of 14 pb^{-1} was accumulated. After a short shutdown, during which also minor repairs on the central silicon tracker (CST) were carried out, the preaccelerators were tuned again for positrons and until the end of 1999 a luminosity of 20 pb^{-1} was available for physics analysis. The run continued with positrons after the christmas break and will only end in September 2000. The big shutdown originally planned for May 2000 has been delayed by four months to let the HERA-B experiment take first physics data, and also adapt for delivery delays of various components needed for the upgrade of HERA, the H1- and the Zeus-experiment. As can be projected from the statistics given in Table 7.1 the available event samples at the end of this run should be about three times larger than what is being used in our publications, which include up to 1997 data.

Table 7.1: *Summary of HERA and H1 operation during the last eight years.*

		e^-p			e^+p			
Parameter		1993/4 1998	1999	Sum	1994 -1997	1999	2000[a]	Sum
Integrated luminosity $\mathcal{L}$								
HERA produced	[pb^{-1}]	10.6	17.7	28.3	68.5	27.3	25.9	121.7
HERA physics	[pb^{-1}]	9.8	16.8	26.6	64.3	25.7	24.6	114.6
H1 taken	[pb^{-1}]	7.6	15.1	22.7	49.3	22.3	20.7	92.3
H1 physics	[pb^{-1}]	5.7	14.2	19.9	44.2	20.9	19.6	84.7
HERA efficiency	[%]	92	95	94	94	94	95	94
H1 efficiency	[%]	58	85	75	69	82	79	74
Average luminosity	[$(\mu b\ s)^{-1}$]	2.13	3.77	3.15	3.41	4.21	5.48	4.03
Peak luminosity	[$(\mu b\ s)^{-1}$]	8.8	12.1	12.1	10.1	12.6	17.9	17.9
Average p current	[mA]	55.4	74.8	67.5	65.6	83.1	82.8	73.2
Average $e^{\pm}$ current	[mA]	14.4	18.8	17.2	24.0	20.2	23.3	23.0
HERA luminosity runs		521	179	700	1132	244	142	1518
Permanent H1 runs	[10^3]	7.1	2.5	9.6	15.0	3.7	2.7	21.4
Average duration	[min]	17	29	20	21	26	26	22

[a]: until April 16, 2000

Since the 1998 data sample is small, and analysis of the 1999 run still in progress, it is the pre-1998 data on which the 16 publications ([1]-[16]) of the collaboration are based. The following principal areas are covered:

- neutral and charged electroweak current cross sections, proton structure functions and parton densities at high momentum transfer Q^2 [12],
- search for states outside the standard model [5, 14],
- photon structure [1, 10, 15],
- parton-fragmentation into multijet final states [3, 6, 9, 13],
- electroproduction of exclusive final states [8, 11], and
- production of heavy quark-antiquark states, of open charm and beauty [2, 4, 7, 16].

We will report below on the analyses in the heavy quark sector (Section 7.4.2) and on the QCD analysis of low Q^2 structure functions (Section 7.4.1), two areas, where there is manifest activity of the University of Zürich group.

Besides the physics analysis, our activities deal with the maintenance, monitoring and calibration of the detector components built in Zürich for the central tracker and the first level trigger of H1. Last year the integration of the CST [17] into the central tracker analysis was of particular importance. The relative alignment of the individual detector ladders within the CST as well as the relative alignment of the CST within the central drift chambers has been finalized to such an extent, that secondary vertices can be searched for in heavy flavour physics analysis. In the course of improving the central tracker codes the central inner z-drift chamber (CIZ) has been recalibrated, too, and its resolution considerably improved. Further details are given in Section 7.4.2.

Most of our effort, however was directed towards our contribution to the upgrade program of the H1-detector.

7.2 Summary of activities related to the H1-upgrade

The investigation of rare processes at the limits of the kinematically accessible range at HERA requires a luminosity upgrade of the machine [18]. The most important aspect of this program is the improvement of the focussing properties near the interaction region of the H1 detector. The luminosity is expected to increase by a factor of seven to $L = 7.4 \times 10^{31}$ $\mathrm{cm}^{-2}\mathrm{s}^{-1}$.

Part of the H1 upgrade plan [19] is the replacement of the existing inner two proportional chambers (CIP) and the inner drift chamber (CIZ) by a new five-layer proportional chamber. The aim of this change is to improve z-vertex triggering and track reconstruction at the trigger level, as well as the rejection of background events. In order to achieve this the number of readout channels both along the z-axis and in azimuthal direction has to be increased. Furthermore implementing five chambers instead of two will provide redundancy and help to resolve ambiguities from the CST. The new CIP will have pad readout in 16 azimuthal sectors. The trigger scheme is based on a projective geometry of the pads along the z-axis, thus requiring a varying number of pads in each layer ranging from 119 to 93 pads for the innermost and outermost layer, respectively. The increased number of readout channels also requires new readout and trigger electronics.

The project is being coordinated by the University of Zürich with ETH Zürich and University of Heidelberg as partners. The ASIC laboratory in Heidelberg develops the amplifier and readout chip CIPix, and the electronics for trigger and data acquisition is a common Heidelberg and Zürich University effort. ETH Zürich is responsible for all components dealing

with the readout of the data at the detector end, and the transport to the electronic trailer via an optical transmission line with drivers and receivers at either end.

The University of Zürich is also responsible for the mechanical design and construction of the multiwire proportional chambers. The high density of readout channels and new front-end electronics made it necessary to build a cylindrical prototype of the chamber closest to the beam for which the space limitations are critical. The construction of this prototype at 1/3 of the full length was finished in July 1999. The construction of the full-length five-layer chambers started in autumn of 1999 and should be completed early 2001 to be ready for the installation in the H1 detector at the end of the HERA shutdown. Further details are given below in Sections 7.3.1 and 7.3.2.

7.3 Construction of the new CIP

7.3.1 Mechanics

The active gap and the length of new CIP will remain unchanged compared to the existing chamber [20] with 6 mm and 2190 mm, respectively. 480 gold plated tungsten wires, 25 μm in diameter, per plane span the full length, but are supported at two points by two glasfiber epoxy rings. The cathode planes are made of Kapton foil coated with graphite on the front (chamber side, surface resistance 500 [k$\Omega/sq.$]) and supporting 5 μm thick copper pads on the back side. The pads are between 18 mm (inner chamber) and 23 mm (outer chamber) wide and divide the circumference of the cylinder into 16 ϕ-sectors. Each pad is contacted from the $-z$ side via a coaxial cable embedded into Rohacell cylinders. This is shown in Figure 7.1. The Rohacell/foil sandwiches and the glasfiber epoxy flanges at the end provide the basic strength and structure for the chamber. Cutting and preparing 8500 cables of individual length and soldering them at each end is the most time consuming part of the construction.

Figure 7.1: *Construction of the cathode plane for the innermost chamber of CIP on the steel mandrils. Seen here are the flange at the $-z$ end from which the coaxial cables fan out to the approximately 1500 cathode pads. The cables are embedded into a Rohacell cylinder.*

The whole package requires four cylinders, which have a cathode readout plane on the inside and a cathode/wire plane on the outside, one cylinder with only a cathode readout plane at the outer radius and one cylinder with only a wire plane closest to the beam. The

first two cylinders of this sequence have been completed. Most geometrical details were first successfully tested with an one-third length full diameter prototype (see Figure 7.2). It continues to serve for tests of the on-chamber electronics and the readout chain.

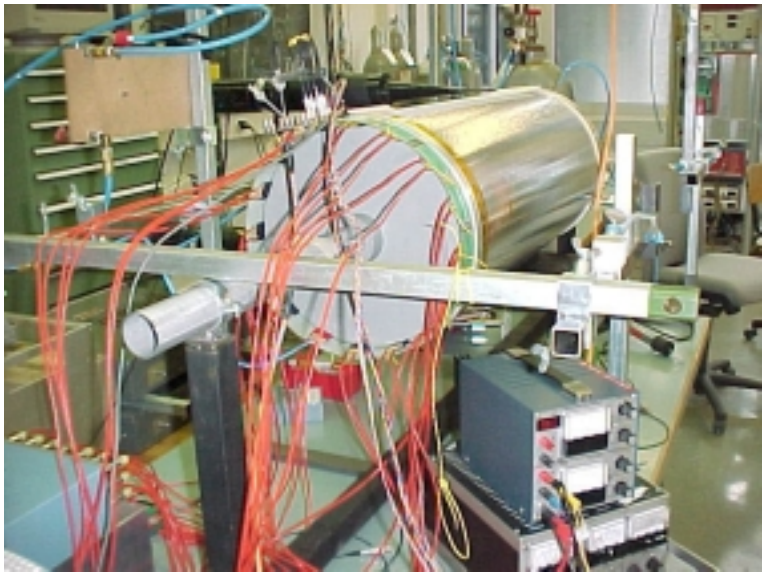

Figure 7.2: *The one-third full length prototype of the new CIP being tested in the laboratory.*

7.3.2 Electronics

The signal readout chain starts on the chamber with the CIPix amplifier chip [21] derived from the HELIX chip [22], which was developed for the HERA-B microstrip gas chambers. The chip contains an integrating preamplifier and shaper for 64 channels, which is followed by a discriminator with a programmable threshold. The digital signals are synchronized with the HERA 10.4 MHz clock and multiplexed fourfold at the output. The analog signal of one channel (programmable) can also be inspected. The programs are loaded via a standard I^2C interface. A small series of prototypes from a multiproject wafer was already available for testing. Figure 7.3 shows CIPix signals recorded with a β source in September 1999 on the CIP prototype. The characteristic Landau-distribution of the pulse height and the exponential dependence of its average on chamber voltage has been verified.

In January 2000 the complete readout chain including the optical transmission line with drivers, 40 m cable and receiver was assembled and has been tested. The digital functions of the CIPix chip are sufficiently well understood, such that final submission could be made.

In the electronics trailer the digital signals from the optical transmission line are handled by one receiver card for two ϕ-sectors. A trigger card deals with all five planes of a given ϕ-sector. The signals are transmitted from the receiver card to the trigger card via the CIP backplane (see Figure 7.4), which requires a rather complicated layout, but does not contain active elements. Four ϕ-sectors require one VME crate, the whole system hence four crates.

All the high level functionality of the system resides in the trigger cards, i.e. the track finding algorithms, the reconstruction of the track origin along the beam axis and the z-vertex histogramming. They contain a complete data acquisition system for all digital signals including a 32 bunch crossing deep pipeline, and the control logic for the VME readout, which requires less than 400 μs. For the first time in a particle physics experiment the whole system is implemented using a new type of FPGA (field programmable gate array, type APEX

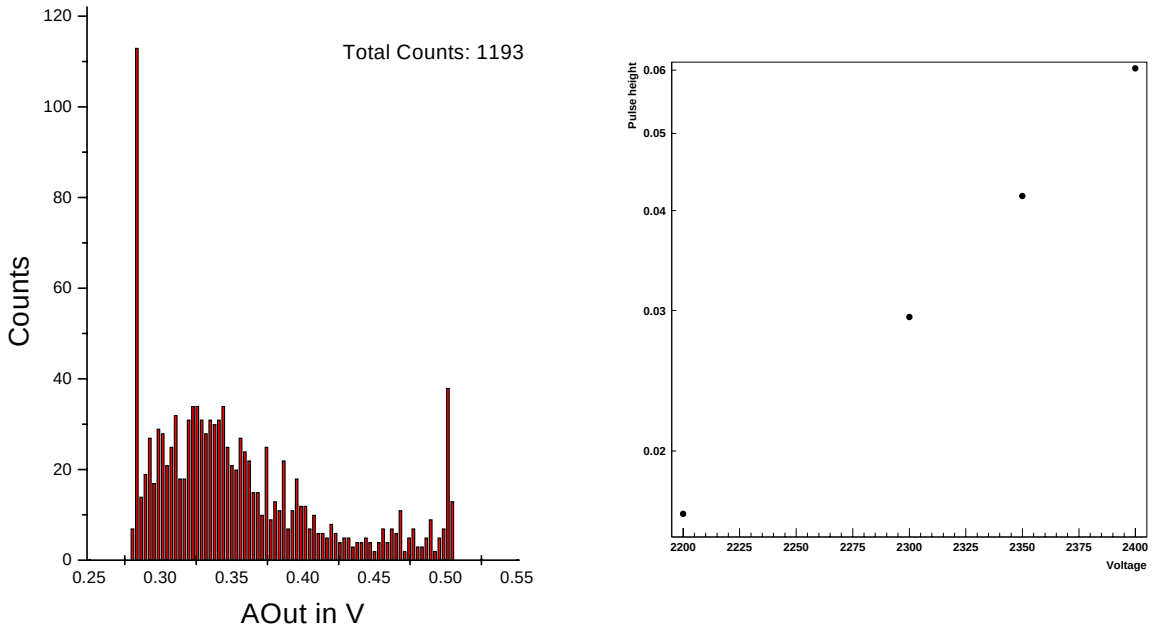

Figure 7.3: *Left: pulse height distribution measured with a* $^{106}_{44}Ru$ *(β^- source) and the CIPix amplifier on the chamber prototype. Right: average pulse height in function of chamber voltage.*

20K400 from ALTERA, available since mid 1999). With up to 500 inputs and outputs, and a large amount of configurable memory aside from the usual logical elements, the use of these circuit elements will allow to build rather complex and still fast trigger systems in the future. Since October 1999 a first, reduced prototype has been in use for tests with different trigger algorithms. The first complete prototype is presently being tested in Heidelberg.

The details of the auxiliary electronics for the distribution of the trigger control signals, HERA clock distribution and control of phase stability with respect to this clock, summation of histograms and production of trigger elements have not been fixed, but the development is in progress.

So far most of the development tasks on the trigger project have been the subject of diploma theses at the University of Heidelberg supervised by U. Straumann. The same holds for the integration of the new system into the existing H1 online system, for which commercial VME processors and VME crate interconnects are foreseen.

7.4 Results from recent analyses

7.4.1 Determination of the gluon density and the strong coupling constant α_s

The measurement of inclusive differential cross sections in ep scattering at HERA provides data for the most complete and accurate test of the dynamics of the strong interaction (QCD) in its perturbative regime. The analysis of the data proceeds in two steps: First the cross section is determined in bins of E'_e, the energy of the scattered electron, and θ, the scattering angle in the laboratory system. Then these data points are fitted with the QCD evolution equation [23] as a function of the Bjorken scaling variable x and the invariant momentum transfer Q^2, resulting in quark and gluon momentum density distributions and the value of the strong coupling constant.

The first step requires detailed understanding of the detector response. Among other con-

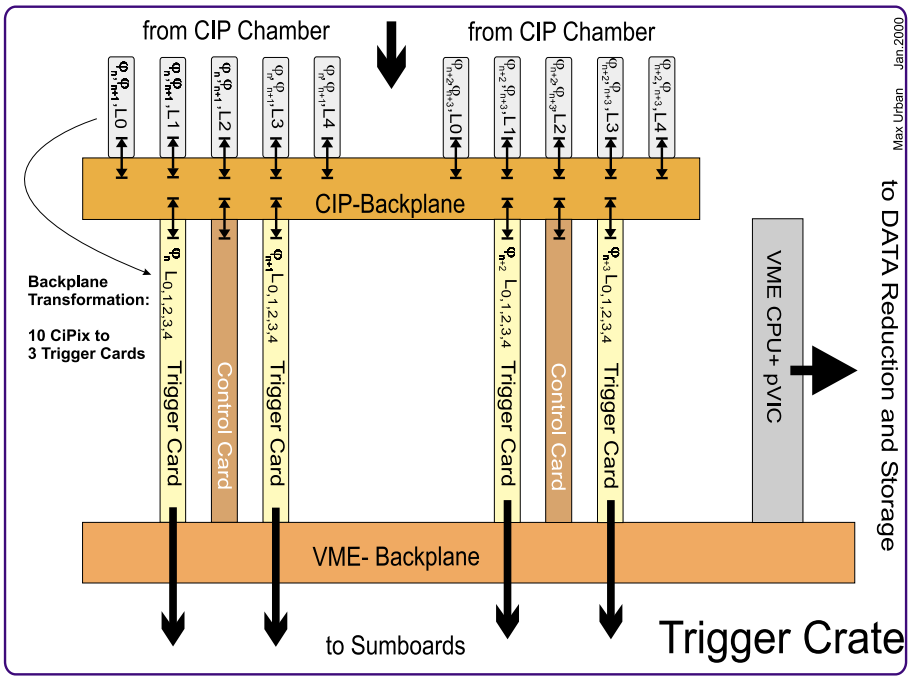

Figure 7.4: *Components for trigger and data acquisition contained in a trigger card, which serves four ϕ-sectors. The custom made CIP backplane resides in the lower part of the crate. The receiver cards are connected to the back side, and the control cards to the front side of this plane. The upper part of the crate contains the standard VME-bus for data transfer, control and monitoring.*

tributions the energy calibration, and the event vertex determination accuracy and efficiency contribute most to the final systematical uncertainties.

Especially difficult is the region, where the electron is only weakly scattered (θ close to π) and is detected in the backward drift chamber (BDC) and the lead - scintillating fiber calorimeter (SPACAL). Both the energy calibration and the determination of the scattering angle by the BDC is spoiled by the fact, that there is a lot of dead material distributed very inhomogeneously in front of these detectors. The thesis project of R. Wallny contains extensive Monte Carlo simulations and comparison to experimental data, which allowed to determine reliable systematical uncertainties in this area. In his diploma work P. Sievers studied different possibilities to correct the energy response of the SPACAL by making use of the charge measurement from the electron showers in the BDC.

Since data taking at very low Q^2 is difficult, due to the overwhelming rate of electron and proton beam induced background in this domain of low electron energy loss and high θ, 1.8 pb^{-1} of luminosity were taken in a special period in autumn 1997 using a dedicated trigger. R. Wallny was the driving force behind this run. He prepared the special trigger conditions, monitored the data quality and adapted the trigger conditions, if necessary.

The second step consists of a QCD evolution analysis in the variables x, Q^2, described by the DGLAP equations [23] in next-to-leading order perturbation theory [23]. Since these equations do not describe the gluon and quark distributions ab initio, assumptions at a given scale Q_0^2 about the shape of these distributions as a function of x have to be made. Since the cross section below $x \approx 10^{-2}$ is dominated by electrons scattered off quarks virtually generated from gluons, this domain is specially sensitive to the gluon distribution. The higher x region is mainly sensitive to the valence quark distributions.

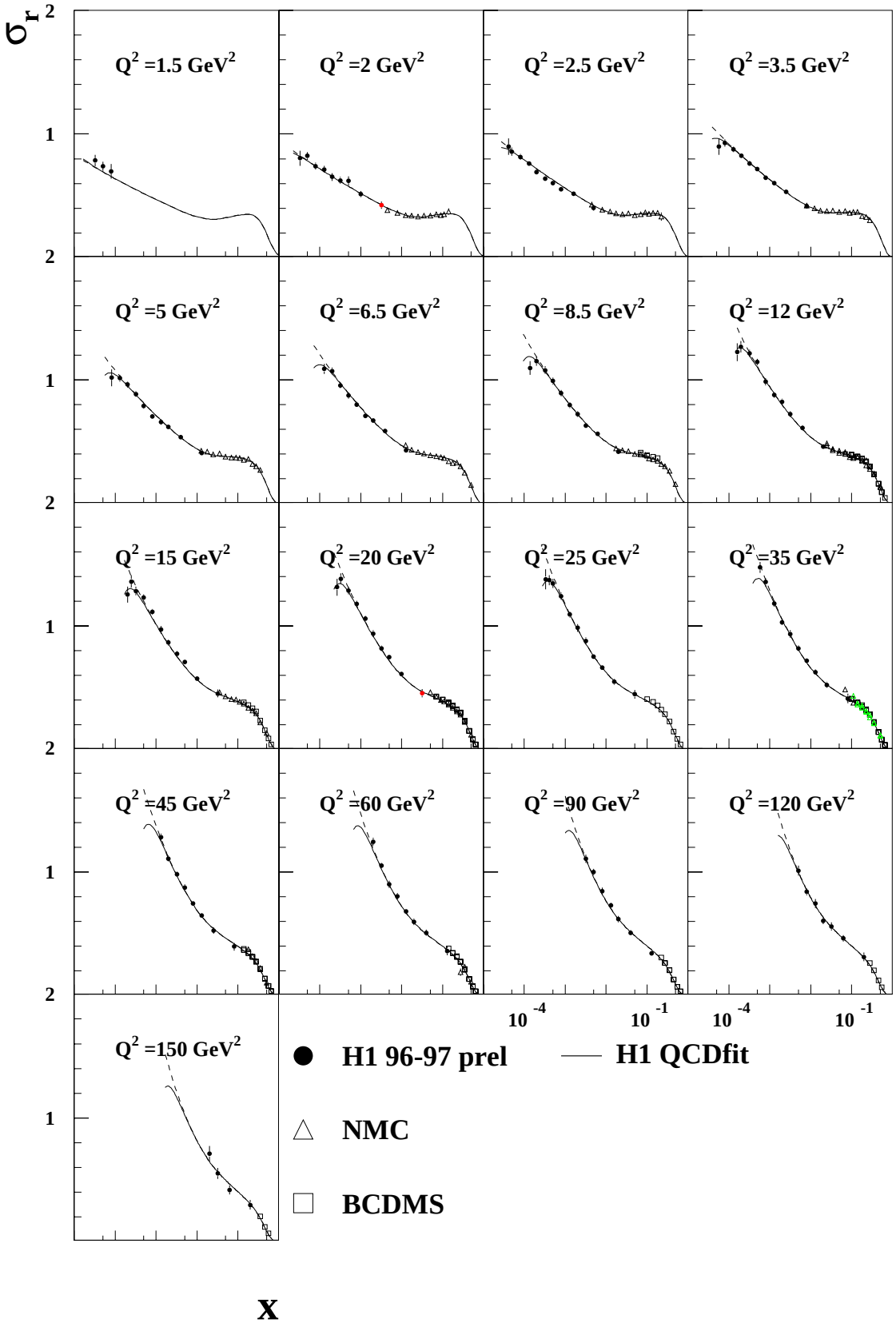

Figure 7.5: *Reduced cross sections σ_r (measured cross section with the trivial kinematical factors divided out) as a function of the Bjorken scaling variable x for different Q^2. The H1 data are compared to data from fixed target μp scattering [24, 25]. The solid line represents the QCD fit based on the H1 data alone.*

In the present analysis also results from NMC [24] and BCDMS [25] are being considered in addition to the H1 data. The analytic form of the parametrisation of the initial parton distributions, the scale Q_0^2 and the coupling constant α_s are varied. Since it is not known, down to what value of Q^2 the perturbative approach of QCD is valid, and since in addition the systematical uncertainties at low Q^2 in all experimental data considered are least well known, all data points below an additional parameter Q_c^2 are not included in the fit. The goal is to find a set of the unphysical parameters Q_0 and Q_c, with which the fit result (the χ^2 distribution) does neither depend on these parameters nor on the experiments included in the fit. Then the fit may give results on the shape of the parton distributions and on the values of α_s.

As an example of such an analysis, Figure 7.5 shows the data points of all three experiment for different Q^2 with the fit superimposed. For the latter only H1 data are used in this case. The fit demonstrates the consistency of the H1 data with those from the other experiments. At very low x and intermediate Q^2 a change in the shape of the cross section can be observed. This is the region, where longitudinally polarized photons start to play a significant role. Figure 7.6 shows the gluon momentum density distributions extracted from this fit for different Q^2.

It is interesting to note, that in contrast to earlier analyses it was not necessary to use deuteron data to pin down the different valence quark distribution, because the accuracy of the H1 data is now sufficient. The momentum sum for all partons has been required in the fits, the resulting total momentum fraction carried by the gluons is about 46%.

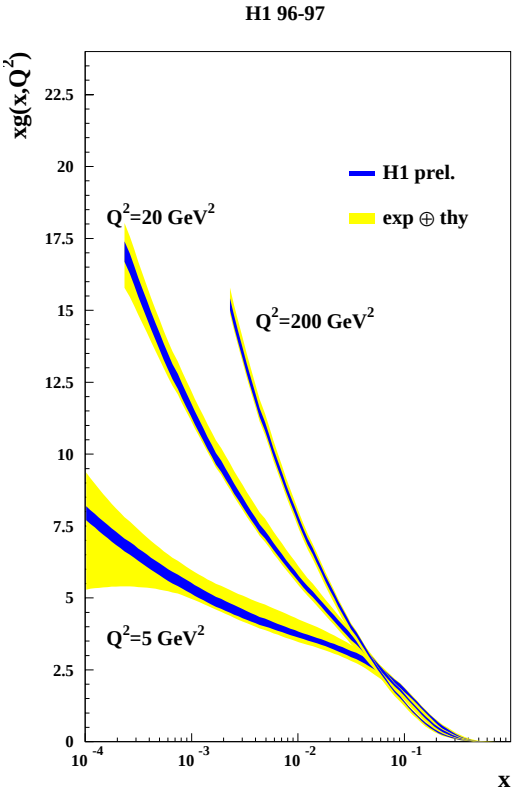

Figure 7.6: *The momentum distribution function of gluons in the proton as observed by ep scattering with different Q^2, and obtained from the results of the QCD fits to the inclusive electron scattering data. The error bands include statistical errors (dark), and uncertainties due to variations of the parameters Q_0, Q_c, α_s, the charm mass as well as uncertainties coming from different parametrisation forms of the light parton distributions.*

7.4.2 Photo- and electroproduction of charm quarks

Heavy flavour physics at HERA focuses on aspects related to production dynamics rather than weak decays and mixing angles. Heavy quarks – like jets – reflect the properties of hard sub-processes in ep interactions. Their mass provides the natural scale which allows the application of perturbative methods in QCD and also testing the theory in regions where no other hard scale (like high transverse energy) is present. Furthermore, when probing the structure of matter, heavy quarks single out the gluonic content.

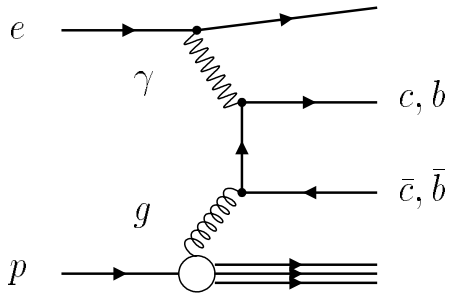

Figure 7.7: *Boson gluon fusion.*

In QCD, c and b production in ep collisions proceed mainly via the boson gluon fusion diagram shown in Figure 7.7. Therefore, charm production has already in the past offered a way to determine the gluon density in the proton. At HERA, this has been performed at low values of the momentum fraction x where the gluon density is steeply rising [2]. The results, which have been reported here earlier, complement the scaling violation analysis of inclusive structure function data [26] and demonstrate the universality of the parton distribution. The concept is also being applied to probe the dynamics of diffractive scattering, mediated via colorless exchange. In a partonic interpretation of the exchanged object (the "Pomeron") charm production is sensitive to its gluon content. The differential cross section data (thesis S. Hengstmann) still have large, mostly statistical, uncertainties, but they have started to discriminate between different theoretical approaches [27] (see last year's report).

In all these studies open charm is detected in the "golden" decay channel $D^{*+} \to D^0\pi^+$ followed by $D^0 \to K^-\pi^+$ which has a favorable signal-to-background ratio, but its fragmentation and decay fraction is only 0.7%. Consequently, not only the diffractive results are statistically limited so far, and important aspects of the theoretical picture in next-to-leading order (NLO) QCD could not yet be addressed. In order to probe the theory beyond the tree level and to measure effects which are absent in leading order (LO), like transverse momentum imbalance or acoplanarity of the produced quark-antiquark pair, both charm quarks need to be tagged. In photoproduction, such "double tags" would allow to clarify the mechanisms of so-called resolved contributions which are still under theoretical debate.

Furthermore higher tagging efficiencies are also needed to explore otherwise unaccessible regions of phase space. It has not yet been possible to measure with sufficient precision the charm contribution to the proton structure function F_2 at higher four-momentum transfers Q^2, where a description in terms of a charm density in the proton – as needed to predict production rates at future colliders – should be adequate. At high Q^2 and p_t, new opportunities will also arise in charged current processes and in the search for new physics.

What holds for charm, is even more true for beauty. Only the inclusive photoproduction cross section could be determined so far [7]; it is about two orders of magnitude smaller than in the charm case, but larger than expected. The measurements to date rely exclusively on the well established signature of semileptonic decays of b hadrons in jets and the higher

transverse momentum p_T^{rel} of the lepton with respect to the jet direction, due to the higher b mass.

The long lifetimes of charm and beauty hadrons which can be measured with micro-vertex detectors provide an independent signature, With its CST the H1-collaboration is for the first time pursuing this direction at HERA.

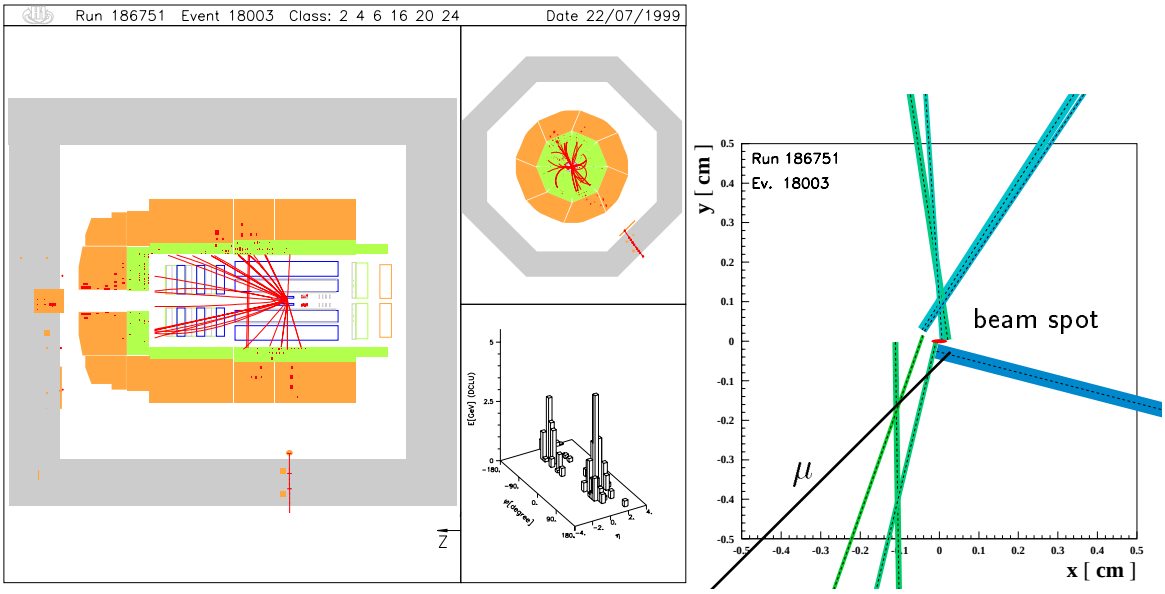

Figure 7.8: *A candidate event for beauty production with subsequent semi-muonic decay. In the magnified view perpendicular to the beam (on the right-hand side) the tracks measured in the CST are represented as bands with widths corresponding to their $\pm 1\sigma$ precision.*

We show here one example from an on-going study (thesis J. Kroseberg) where charm and beauty quarks are identified by means of their semileptonic decays. An event with two jets and a penetrating track identified as a muon is shown on the left-hand side of Figure 7.8. The muon has a relatively high transverse momentum of 3 GeV/c with respect to the nearest jet, which is unlikely for muons from charm decays or misidentified hadrons but is expected for decays of b flavoured hadrons, due to their higher mass. In the magnified view perpendicular to the beam (on the right-hand side) the tracks measured in the CST are represented as bands with widths corresponding to their $\pm 1\sigma$ precision. The resolution provided by the CST reveals that the muon track originates from a well separated secondary vertex. The distribution of impact parameters, defined as the distance of closest approach between the muon tracks and the interaction vertex, signed positive when the intercept of the track with the jet axis lies behind the interaction vertex (along the jet direction), and negative otherwise, is plotted in Figure 7.9. Positive impact parameters are a signature of decays of short-lived particles, and the clearly visible asymmetry of the distribution provides a measure of the charm and beauty content of the event sample. This analysis is a pioneering project which could become one of the first physics results obtained with a Silicon vertex detector at HERA. The work therefore presently has an emphasis on technical aspects and involves the development of track reconstruction software and analysis tools.

The lifetime signature is in principle present in every event and has in fact been exploited successfully as heavy quark tag with highest efficiency in many other experiments to-date. The b-enriched sample and the clear event topology of the muon analysis provide an optimal testing ground for such techniques. The extension to the general case including hadronic

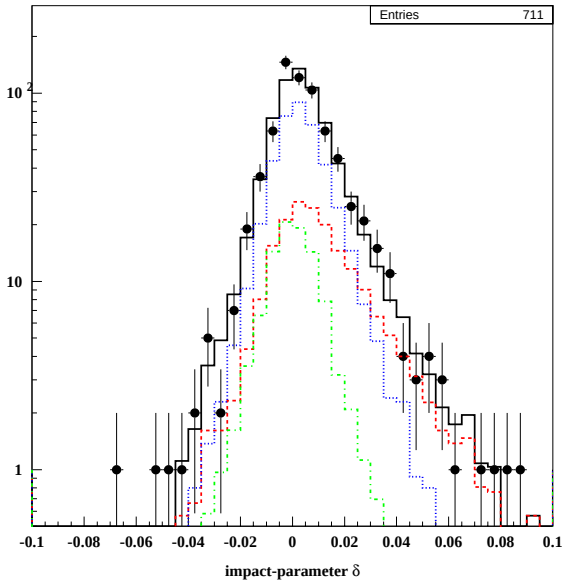

Figure 7.9: *Impact parameter distribution for muon candidate tracks in di-jet events. The histogram is the superposition of Monte Carlo predictions for $b\bar{b}$ production (dashed), $c\bar{c}$ production (dotted), and mis-identified hadrons (dash-dotted).*

decays is presently being studied using Monte Carlo simulations (thesis I. Foresti). A simple and robust method is to combine the information contained in the impact parameters of all tracks with sufficient momentum, and to derive an estimate of secondary vertex activity in the event.

Not relying anymore on exclusive signatures (like a muon) puts additional strain on the tracking precision requirements, because non-Gaussian measurement errors compete with the low signal-to-background ratio. The full potential of the CST can only be realized with optimized performance and consistency of the entire tracking system. Here, the CST, in turn, together with new numerical methods, provides new handles for calibration and alignment of the outer tracking detectors. A collaboration-wide effort has been initiated to lift the tracking performance to the standards of micro-vertexing methods (F. Sefkow acts as a convener of this new group).

For example (thesis S. Hengstmann), it has now become both necessary and possible to achieve higher precision in the central inner z-chamber (CIZ), built at our institute. Optimal track precision in the z direction is important to minimize the wrong assignment of noise hits from the CST z measurement to track candidates. Using a large sample of cosmic events, correction constants have been determined for each single wire. With such a calibration, the hit resolution has already been improved from 800 μm to 500 μm. With precise CST tracks as reference, further corrections can be applied, resulting in a further improvement to 360 μm, which is now consistent with the intrinsic resolution of the chamber, as determined from hit triplets. Benefits from such progress can be expected in a large variety of physics applications, ranging from the mostly track-based heavy quark analyses to better reconstruction of event kinematics at very high Q^2.

References

[1] *Charged Particle Cross Sections in Photoproduction and Extraction of the Gluon Density in the Photon*,
H1-Collaboration, C. Adloff *et al.*, Eur. Phys. J. **C10** (1999), 363.

[2] *Measurement of D^* Meson Cross Sections at HERA and Determination of the Gluon Density in the Proton*,
H1-Collaboration, C. Adloff *et al.*, Nucl. Phys. **B545** (1999), 21.

[3] *Measurement of Internal Jet Structure in Di-jet Production in Deep Inelastic Scattering at HERA*,
H1-Collaboration, C. Adloff *et al.*, Nucl. Phys. **B545** (1999), 3.

[4] *Charmonium Production in Deep Inelastic Scattering at HERA*,
H1-Collaboration, C. Adloff *et al.*, Eur. Phys. J. **C10** (1999), 373.

[5] *A Search for Leptoquark Bosons and Lepton Flavour Violation in e^+p Collisions at HERA*,
H1-Collaboration, C. Adloff *et al.*, Eur. Phys. J. **C11** (1999), 447.

[6] *Measurement of Transverse Energy Flow in Deep-Inelastic Scattering at HERA*,
H1-Collaboration, C. Adloff *et al.*, Eur. Phys. J. **C12** (2000), 595.

[7] *Measurement of Open Beauty Production at HERA*,
H1-Collaboration, C. Adloff *et al.*, Phys. Lett. **B467** (1999), 156.

[8] *Forward π^0-Meson Production at HERA*,
H1-Collaboration, C. Adloff *et al.*, Phys. Lett. **B462** (1999), 440.

[9] *Di-jet Rates in Deep-Inelastic Scattering at HERA*,
H1-Collaboration, C. Adloff *et al.*, Eur. Phys. J. **C13** (2000), 415.

[10] *Measurement of Di-jet Cross Sections in Low Q^2 and the Extraction of an Effective Parton Density for the Virtual Photon*,
H1-Collaboration, C. Adloff *et al.*, Eur. Phys. J. **C13** (2000), 397.

[11] *Elastic Electroproduction of ρ Mesons at HERA*,
H1-Collaboration, C. Adloff *et al.*, Eur. Phys. J. **C13** (2000), 371.

[12] *Measurement of Neutral and Charged Current Cross Sections in Positron-Proton Collisions at Large Momentum Transfer*,
H1-Collaboration, C. Adloff *et al.*, DESY 99 – 107, hep-ex 9908059, Eur. Phys. J. **C** (2000), in print.

[13] *Investigation of Power Corrections to Event Shape Variables Measured in Deep-Inelastic Scattering*,
H1-Collaboration, C. Adloff *et al.*, DESY 99 – 193, hep-ex 9912052, Eur. Phys. J. **C** (2000), in print.

[14] *Search for Compositeness, Leptoquarks and Large Extra Dimensions in eq Contact Interactions at HERA*,
H1-Collaboration, C. Adloff *et al.*, DESY 00 – 027, hep-ex 0003002, subm. to Phys. Lett. **B** (2000).

[15] *Measurement of Di-jet Cross Sections in Photoproduction and Photon Structure*,
H1-Collaboration, C. Adloff *et al.*, DESY 00 – 035, hep-ex 000311, subm. to Phys. Lett. **B** (2000).

[16] *Elastic Photoproduction of J/Ψ and Y Mesons at HERA*,
H1-Collaboration, C. Adloff *et al.*, DESY 00 – 037, hep-ex 000320, subm. to Phys. Lett. **B** (2000).

[17] *The H1 Silicon Vertex Detector*,
D. Pitzl, O. Behnke, M. Biddulph, K. Bösiger, R. Eichler, W. Erdmann, K. Gabathuler, J. Gassner, W.J. Haynes, R. Horisberger, M. Kausch, M. Lindström, H. Niggli, G. Noyes, P. Pollet, S. Steiner, S. Streuli, K. Szeker, and P. Truöl, hep-ex 0002044, subm. to Nucl. Instr. Meth. **A** (2000).

[18] *ep physics beyond 1999*,
H1 note H1-10/97-531, April 1998.

[19] *H1 high luminosity upgrade 2000: CIP and level-1 vertex trigger*,
M. Cuje *et al.*, H1 note H1-01/98-539, January 1998.

[20] K. Müller *et al.*, Nucl. Instr. Meth. **A312** (1992) 457.

[21] CIPix User Manual: *http://wwwasic.ihep.uni-heidelberg.de /h1cip/CIPix_manual/CIPix_UserManual.v1_0.html*

[22] HELIX User Manual: *http://wwwasic.ihep.uni-heidelberg.de /~feuersta/projects/Helix/index.html*

[23] Yu.L. Dokshitzer, Sov. Phys. JETP **46** (1977) 641;
V.N. Gribov, and L.N. Lipatov, Sov. J. Nuc. Phys. **15** (1972) 438 and 675;
G. Altarelli, and G. Parisi, Nucl. Phys. **B126** (1977) 298.

[24] NMC-Collaboration: M. Arneodo *et al.*, Phys. Lett. **B364** (1996) 107.

[25] BCDMS-Collaboration: A.C. Benvenuti *et al.*, Phys. Lett. **B223** (1989) 485.

[26] H1-Collaboration, S. Aid *et al.*, Nucl.Phys. **B470** (1996) 3.

[27] S. Hengstmann, Nucl. Phys. (Proc. Suppl.) **B79** (1999) 296.